AMERICAN SOCIETY FOR MICROBIOLOGY | Journal of Virology®

STRUCTURE AND ASSEMBLY

N-Linked Glycan Sites on the Influenza A Virus Neuraminidase Head Domain Are Required for Efficient Viral Incorporation and Replication

Henrik Östbye,[a] Jin Gao,[b] Mira Rakic Martinez,[b] Hao Wang,[a] Jan-Willem de Gier,[a] Robert Daniels[b]

[a]Department of Biochemistry and Biophysics, Stockholm University, Stockholm, Sweden
[b]Division of Viral Products, Center for Biologics Evaluation and Research, Food and Drug Administration, Silver Spring, Maryland, USA

ABSTRACT N-linked glycans commonly contribute to secretory protein folding, sorting, and signaling. For enveloped viruses, such as the influenza A virus (IAV), large N-linked glycans can also be added to prevent access to epitopes on the surface antigens hemagglutinin (HA or H) and neuraminidase (NA or N). Sequence analysis showed that in the NA head domain of H1N1 IAVs, three N-linked glycosylation sites are conserved and that a fourth site is conserved in H3N2 IAVs. Variable sites are almost exclusive to H1N1 IAVs of human origin, where the number of head glycosylation sites first increased over time and then decreased with and after the introduction of the 2009 pandemic H1N1 IAV of Eurasian swine origin. In contrast, variable sites exist in H3N2 IAVs of human and swine origin, where the number of head glycosylation sites has mainly increased over time. Analysis of IAVs carrying N1 and N2 mutants demonstrated that the N-linked glycosylation sites on the NA head domain are required for efficient virion incorporation and replication in cells and eggs. It also revealed that N1 stability is more affected by the head domain glycans, suggesting N2 is more amenable to glycan additions. Together, these results indicate that in addition to antigenicity, N-linked glycosylation sites can alter NA enzymatic stability and the NA amount in virions.

IMPORTANCE N-linked glycans are transferred to secretory proteins upon entry into the endoplasmic reticulum lumen. In addition to promoting secretory protein maturation, enveloped viruses also utilize these large oligosaccharide structures to prevent access to surface antigen epitopes. Sequence analyses of the influenza A virus (IAV) surface antigen neuraminidase (NA or N) showed that the conservation of N-linked glycosylation sites on the NA enzymatic head domain differs by IAV subtype (H1N1 versus H3N2) and species of origin, with human-derived IAVs possessing the most variability. Experimental analyses verified that the N-linked glycosylation sites on the NA head domain contribute to virion incorporation and replication. It also revealed that the head domain glycans affect N1 stability more than N2, suggesting N2 is more accommodating to glycan additions. These results demonstrate that in addition to antigenicity, changes in N-linked glycosylation sites can alter other properties of viral surface antigens and virions.

KEYWORDS IAV composition, NA, N-linked glycosylation sites, glycoprotein maturation, stability, surface antigen, viral replication

Glycoproteins receive N-linked glycans when they are inserted into the endoplasmic reticulum (ER) lumen. The addition of these large oligosaccharide structures can lower the activation barrier for the glycoprotein to fold, and they can function as docking sites for cellular factors that assist in the folding, quality control, and trafficking of the newly synthesized glycoprotein (1–4). Following the maturation process,

Citation Östbye H, Gao J, Martinez MR, Wang H, de Gier J-W, Daniels R. 2020. N-linked glycan sites on the influenza A virus neuraminidase head domain are required for efficient viral incorporation and replication. J Virol 94: e00874-20. https://doi.org/10.1128/JVI.00874-20.

Editor Stacey Schultz-Cherry, St. Jude Children's Research Hospital

Address correspondence to Robert Daniels, Robert.Daniels@fda.hhs.gov.

Received 6 May 2020
Accepted 15 July 2020
Accepted manuscript posted online 22 July 2020
Published 15 September 2020

N-linked glycans can also contribute to the function of the glycoprotein by influencing local conformations, extending the half-life, or directly participating in critical protein interactions (5–9). Many envelope viral glycoproteins utilize N-linked glycans for these common cellular functions (10–12) and for the ability of the large glycan structures to limit access to sensitive epitopes (13–17). For influenza viruses, the roles of N-linked glycans in the folding and masking of epitopes on its surface glycoprotein hemagglutinin (HA or H) have been well-established (13, 18–20). However, a comprehensive picture is lacking for how N-linked glycans contribute to the other influenza glycoprotein, neuraminidase (NA or N), as only a few experimental studies have been performed (17, 21).

The HA and NA glycoproteins from influenza A viruses (IAVs) are quite diverse and are classified into subtypes based on their antigenic and genetic properties (22). Presently, 16 HA (designated H1 to H16) and nine NA (designated N1 to N9) subtypes have been identified in avian IAVs in almost every possible combination (23). Despite this variability, only H1N1 and H3N2 subtypes seasonally circulate in the human population, and they are also commonly isolated from swine species, which are susceptible to both avian and human IAVs (24, 25).

There are some similarities between the numerous NA subtypes. All are type II membrane glycoproteins that form a Ca^{2+}-dependent tetrameric enzyme (26–30). The enzymatic function, located in the C-terminal head domain, promotes the mobility of the virus by removing the terminal sialic acid residues that HA binds to on host and viral glycan structures (31, 32). Synthesis of NA is dependent on the 5′ region of its mRNA, which codes for an N-terminal transmembrane domain of varying hydrophobicity that cotranslationally targets NA to the ER (27, 33–35). The transmembrane domain then inverts and integrates into the ER membrane as the C-terminal stalk and head domain are synthesized and translocated into the ER lumen (34). Upon entering the Ca^{2+}-rich ER lumen, the stalk and the enzymatic head domain receive multiple N-linked glycans that are capable of recruiting chaperones (21, 36). The chaperones likely assist in the folding and oligomerization of NA, which occurs through a cooperative process that involves the enzymatic head and the distal transmembrane domain (21, 37–39).

Previous work focused on the N-linked glycans of NA showed that an avian N9 variant predominantly misfolds in CHO cells when not glycosylated and that the misfolding is mainly caused by the loss of the head domain glycans (21). More recent studies on H1N1 IAVs have begun to examine the temporal frequency of N-linked glycosylation sites in N1 (40–42) and the heterogeneity of the N-linked glycan structures (36). The positional analysis has led to the speculation that many N1 glycan sites correlate with antigenic regions (41), whereas the glycan analysis identified a single site on the N1 head domain that is modified by a wide variety of glycans, with a diverse antenna array when expressed in eggs (36). However, the impact of these sites on NA has not been looked at directly for H1N1 IAVs, and even less data are available for these sites from H3N2 IAVs.

Here, we examined the glycosylation site frequencies in the NA sequences from H1N1 and H3N2 strains by domain (stalk versus head), year of isolation, and species of origin. Three conserved sites were identified in the N1 head domain and four in the N2 head domain. For the N1 head domain, variable glycosylation sites are almost exclusive to human H1N1 IAVs, whereas the N2 head domain has more variable sites, and these are present in human, swine, and avian H3N2 IAVs. Analysis of viruses carrying NAs with mutated glycosylation sites revealed that the ones in the head domain are required for efficient virion incorporation and replication and influence NA stability in a subtype-dependent manner. These results illustrate how N-linked glycans on NA can perform multiple functions and may explain why variable glycosylation sites are more prevalent in N2.

RESULTS

Analysis of the N-linked glycan sites encoded by the NA from H1N1 IAVs. N-linked glycans are transferred to the Asn in the consensus sequence N-X-S/T-X, where

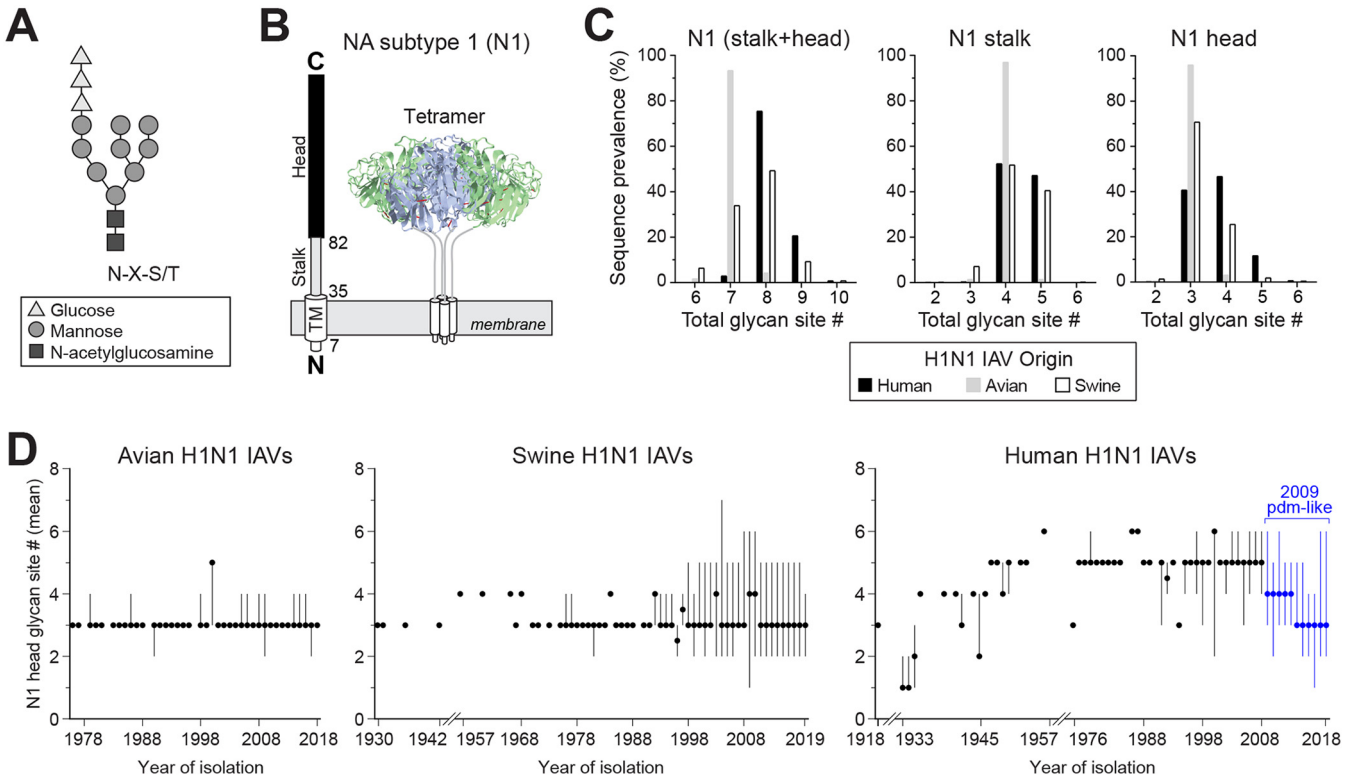

FIG 1 N-linked glycan site variation in NA from H1N1 IAVs by species of origin and time. (A) Diagram of an N-linked glycan structure that is transferred to secretory glycoproteins during entry into the ER lumen. The glycan is added to the Asn (N) of the consensus sequence N-X-S/T. (B) Linear and structural organization of the domains in NA from H1N1 IAVs. The numbers correspond to the amino acid position at the start of the transmembrane (TM), stalk, and head domains of these NAs. (C) Graphs showing the prevalence of the N1 sequences from human (n = 18,966), swine (n = 4,949), and avian (n = 630) H1N1 IAVs that possess the indicated number of glycosylation sites in the stalk and head domain (left), the stalk alone (middle), and the head domain alone (right). (D) Temporal graphs displaying the mean number of glycosylation sites in the N1 head domain with respect to the year the avian (left), swine (middle), and human (right) H1N1 IAVs were isolated. Filled circles correspond to the means, and those in blue (right) indicate strains derived from the 2009 pandemic H1N1 IAV of Eurasian swine origin. Lines show the range in the number of sites in the sequence set for each year. All analyses were performed using full-length NA sequences downloaded from the NCBI Influenza Database.

X can be any amino acid other than Pro (43, 44). The addition of the glycan occurs on the luminal side of the ER membrane (Fig. 1A), limiting the accessibility of some regions in membrane proteins. Influenza NA is synthesized as a type II membrane glycoprotein with the N terminus in the cytosol and a long C-terminal region in the ER lumen (Fig. 1B). The C-terminal region contains the stalk and head domain, and both of these regions have been shown to code for multiple N-linked glycosylation sites (21, 34, 40–42). To determine if the glycosylation sites in NA have a domain or temporal bias with respect to the IAV species of origin, we initially examined the available subtype 1 (N1) sequences from H1N1 IAVs. The sequence analysis showed that the majority (~92%) of avian N1s possess seven predicted N-linked glycan sites, whereas the human and swine N1s tend to have more sites and vary in the site number (Fig. 1C, left). In the stalk, most avian N1s have four sites, and the human and swine N1s mainly carry four or five (Fig. 1C, middle). In the head domain, avian N1s predominantly have three sites, whereas the swine N1s contain either three or four and the human N1s range from three to five (Fig. 1C, right). In line with previous reports (40, 42), these differences indicate that the stalk and head domain both contribute to the species-related variation in the number of NA glycosylation sites, but it remains unclear if the bias relates to how the sequences were collected.

Some glycosylation sites in the NA head have been linked to antigenicity (17); therefore, we performed a temporal analysis of the sites in the N1 head domain. Regardless of the year the strain was isolated, the avian N1 head domains were found to mainly contain three sites (Fig. 1D, left), and the swine N1 head domains fluctuated

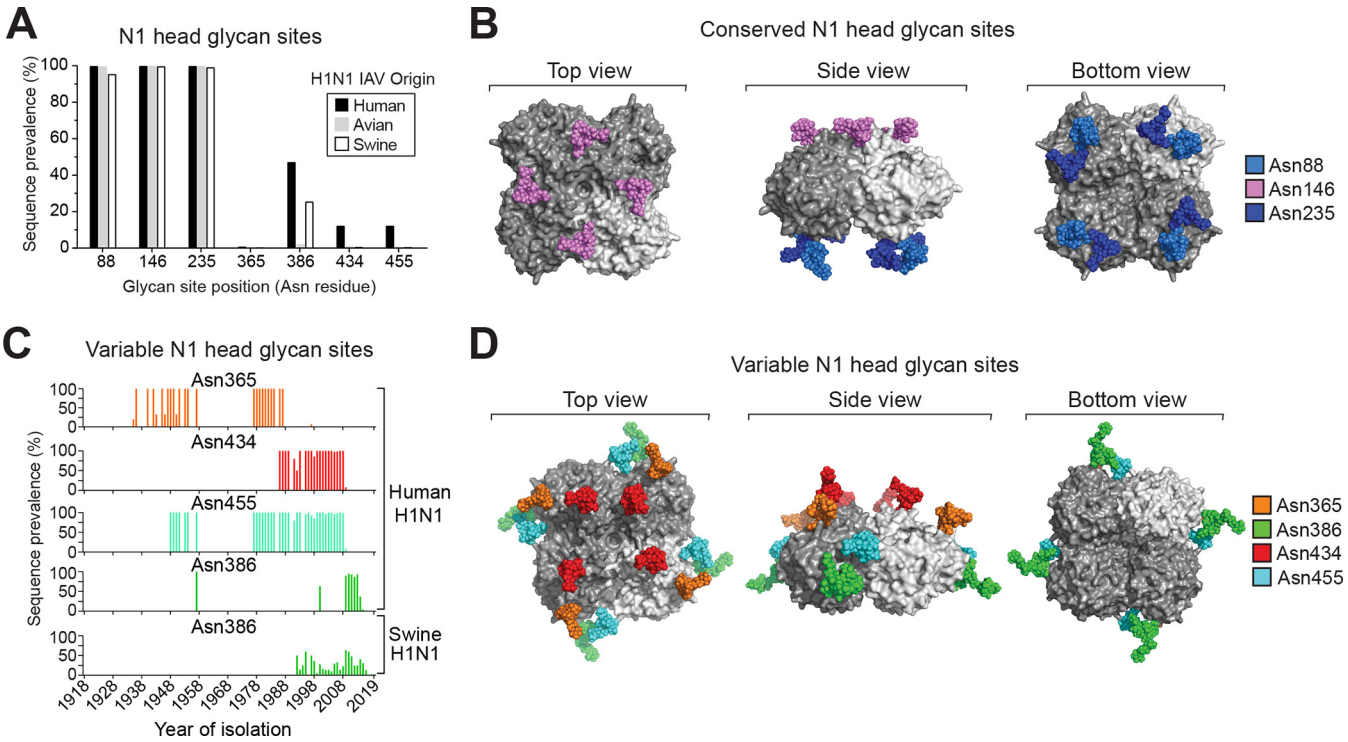

FIG 2 Positions of the N-linked glycan sites in the NA head domain from H1N1 IAVs. (A) Graph showing the prevalence of the most frequent head domain glycosylation sites in the N1 sequences based on the H1N1 IAV species of origin. The positioning refers to the Asn (N) in the N-X-S/T sequence. (B) *In silico* model of N-linked glycan structures mapped onto the conserved sites of a 2009 pandemic-like N1 head domain structure (PDBID entry 5NWE) (59). (C) Temporal graphs displaying the frequency of the most prevalent variable glycosylation sites in the head domain of N1 with respect to the year the sequences were isolated. (D) *In silico* model of N-linked glycans mapped onto a N1 head domain structure (PDBID entry 5NWE) (59) at amino acids that correspond to the position of the prevalent variable head glycosylation sites.

between three and four sites with no temporal pattern (Fig. 1D, middle). In contrast, the human N1 head domains showed a stepwise pattern, with the early strains increasing in the number of sites from three to six and the more recent 2009 H1N1 pandemic-like strains of Eurasian swine origin decreasing from four to three (Fig. 1D, right). These temporal observations indicate that the addition and removal of N-linked glycan sites in the N1 head domain is more characteristic of human H1N1 IAVs and that N1 likely requires at least three glycosylation sites in the head domain.

Location of the N-linked glycan sites in the NA head domain of H1N1 IAVs. Positional analysis revealed that three N-linked glycosylation sites are highly conserved in the N1 head domain in H1N1 IAVs (Fig. 2A). *In silico* modeling of minimal glycan structures onto these sites showed that one (Asn146) is positioned on the top of the NA tetramer and the other two (Asn88 and Asn235) are located close together on the bottom, facing the viral membrane (Fig. 2B). One of the four prevalent variable sites in the human N1 head domain (Asn386) is also frequently found in the swine N1 head domain (Fig. 2C), likely due to the swine origin of the human 2009 pandemic H1N1 virus. Temporally, the prevalent variable sites overlap for different time periods, contributing to the discrete changes observed in the number of glycosylation sites on the human N1 head domain (Fig. 2C and 1D, right). Positionally, three of the variable sites (Asn365, Asn386, and Asn455) cluster toward the NA tetramer side (Fig. 2D), which previously was shown to be an antigenic region in NA (45). The final prevalent variable site at Asn434 is located very close to the conserved site at Asn146 (Fig. 2D), suggesting these two sites, and possibly the other two conserved sites (Asn88 and Asn235), perform redundant roles.

The conserved N1 head glycosylation sites are not essential for viral replication in cells. Although the glycosylation sites at Asn88, Asn146, and Asn235 are highly conserved in the N1 head domain (Fig. 3A), we were able to identify sequences that

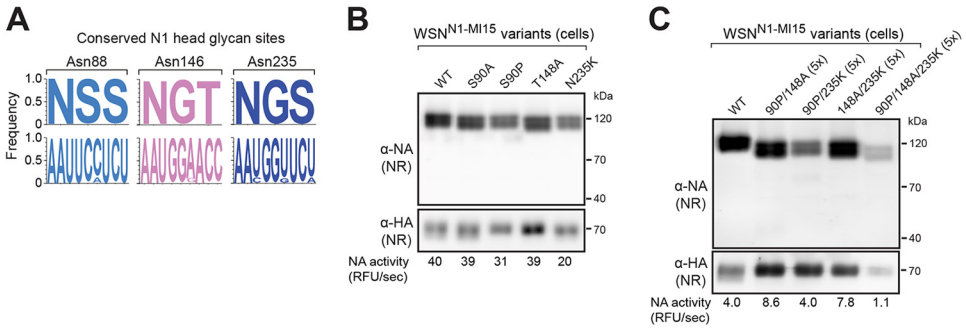

FIG 3 Conserved N1 head glycosylation sites are not essential for viral replication in cells. (A) Logo plots displaying the amino acid (top) and nucleotide (bottom) frequency for the three conserved glycosylation sites on the N1 head domain from human H1N1 IAVs. (B and C) Representative NA and HA immunoblots of recombinant WSN viruses carrying N1-MI15 with the indicated glycosylation site mutations. The viruses were rescued by reverse genetics and passaged in MDCK cells, and the virus-containing supernatants were sedimented and resuspended in equal volumes. Each sample was split, one part was resolved by nonreducing (NR) SDS-PAGE prior to immunoblotting, and the other was used to determine the NA activity values, which are listed below the blots. (C) Samples containing resuspension volumes greater than the WT control are indicated as a ratio in parentheses.

carry a mutation in one of the sites (S90P, T148A, and N235K). These natural mutations were introduced into an NA (N1-MI15) from a previously recommended 2009 pandemic-like H1N1 vaccine strain (A/Michigan/45/2015) in various combinations to determine if the conserved sites are required for H1N1 IAV replication. We chose N1-MI15 for the analysis, as it does not contain any variable head glycan sites. An additional mutation (S90A) was also included to alleviate potential folding concerns associated with the S90P mutation that introduces a Pro residue.

Surprisingly, all the recombinant viruses carrying the N1-MI15 single, double, and triple glycan site mutants were rescued using a WSN33 backbone. These single-gene reassortant viruses, along with an N1-MI15 wild-type (WT) control, were propagated in MDCK cells, isolated by sedimentation, and analyzed. Each of the N1-MI15 variants in the sedimented virions possessed enzymatic activity and resolved as intermolecular disulfide-bonded dimers following nonreducing (NR) SDS-PAGE (Fig. 3B and C), which is a characteristic of properly folded N1 (26, 37). The expected mobility increase was more pronounced for N1-MI15 with the triple and double glycosylation site mutants than for the single-site mutants (Fig. 3B and C), implying the appropriate glycans were absent in the mutants. We also noted that visualization of the double and triple glycan site mutants required higher volumes of the sedimented virus-containing medium (Fig. 3C), suggesting the absence of several conserved glycans modestly impairs viral growth by decreasing NA folding or trafficking.

The conserved N1 head glycosylation sites are not essential for viral replication in eggs. Several factors can potentially influence the results obtained after the conserved glycan sites were mutated in N1-MI15, including the use of the natural mutations, the particular NA, the viral backbone, and the growth environment. Therefore, we repeated the analysis with an NA (N1-BR18) from a more recently recommended 2009 pandemic-like H1N1 vaccine strain (A/Brisbane/02/2018) using a different mutation strategy (N to Q), backbone (PR8), and growth environment (embryonated eggs). Like the prior results, all the recombinant viruses carrying N1-BR18 with single, double, and triple mutations in the head glycan sites were rescued. Upon passaging in eggs, lower hemagglutinating unit (HAU) titers were observed only for the two double glycan site mutants lacking the Asn146 site and the triple glycan site mutant (Fig. 4A, upper graph). Variable NA activity was measured in the egg allantoic fluid for all the viruses apart from the triple glycan site mutant, which consistently produced lower activity levels (Fig. 4A, lower graph). Each of the N1-BR18 mutants displayed increased mobility on reducing (RD) and NR SDS-PAGE, which correlated with the number of glycosylation site mutations (Fig. 4B), indicating the mutations remained intact. Together, these results demonstrate that the conserved N-linked glycosylation sites on the N1 head

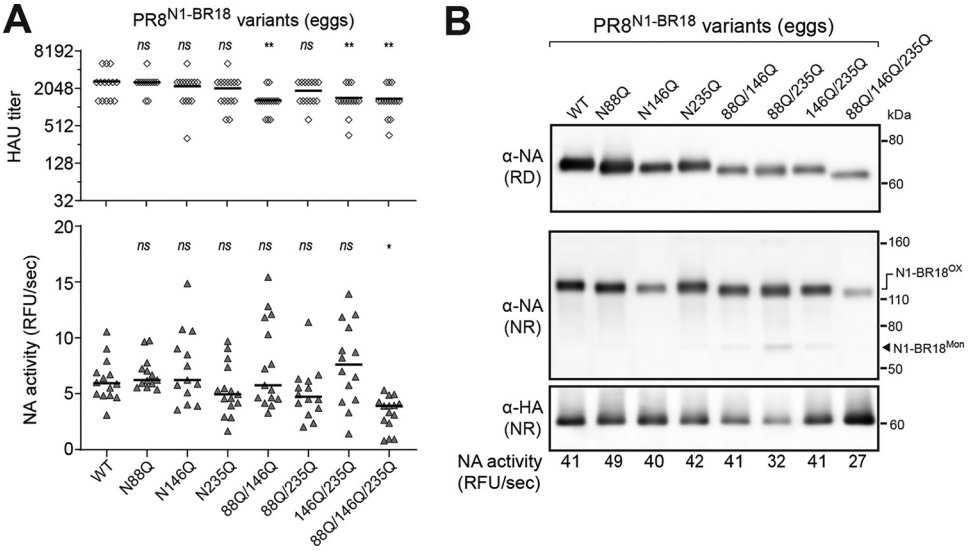

FIG 4 Mutation of the conserved N1 head glycosylation sites causes slight viral replication defects in eggs. (A) Scatterplots of the HAU titers and NA activities that were measured in the allantoic fluid harvested from eggs infected with recombinant PR8 viruses carrying N1-BR18 with the indicated glycosylation site mutations. The viruses were rescued by reverse genetics and passaged twice in eggs. The data points from individual eggs following the second passage are shown together with the medians (line). *P* values (95% confidence interval [CI]) were determined with respect to the WT values by a one-way analysis of variance (ANOVA). (B) Representative NA and HA immunoblots of the recombinant PR8$^{N1\text{-}BR18}$ viruses with the indicated mutations in the N1 head glycosylation sites. The allantoic fluid from the second passage was pooled, and the virions were isolated by centrifugation and adjusted to equal total protein concentrations prior to being resolved by NR and reducing (RD) SDS-PAGE. NA activity (below the immunoblots) in the virions was also measured using equal total protein amounts.

domain are not essential for H1N1 virus replication in cells or embryonated eggs. However, we did observe that viral replication appears to decrease when the three conserved head glycan sites are mutated (Fig. 4A) and that N1 intermolecular disulfide bond formation and virion incorporation are less efficient when two or more glycan sites are absent (Fig. 4B).

The conserved glycans on the head domain influence N1 viral incorporation. When the three conserved glycan sites in the N1-BR18 head domain were mutated, the PR8 backbone virus showed a tendency in eggs to reach lower HAU titers and NA activity levels (Fig. 4A). This raised several questions: is the phenotype backbone dependent, do the mutations change the HA to NA ratio in the virions, or do they cause a decrease in viral production? To address these questions, we rescued a wild-type N1-BR18 virus (WT) and a mutant containing no head glycosylation sites (NHG 3Q) using a WSN backbone. Upon passaging in eggs, both the HAU titer and the NA activity in the allantoic fluid were significantly lower when the three conserved glycosylation sites on the N1 head domain were mutated (Fig. 5A, compare WT to NHG 3Q), demonstrating the phenotype is conserved and may be somewhat exacerbated with a WSN backbone.

The lower HAU titers for the virus carrying the N1-BR18 mutant (NHG 3Q) indicated that the conserved glycosylation sites on the N1 head domain contribute to viral production. To address if the mutations changed the HA to NA ratio in the virus, we isolated the virions by centrifugation and examined equal quantities of total protein by SDS-PAGE followed by Coomassie staining. In the absence of the reductant dithiothreitol (DTT), oxidized N1-BR18 dimers were readily apparent for the WT virus, and these were reduced to the expected molecular weight upon DTT addition (Fig. 5B). Despite the relatively equivalent levels of HA, NP, and M1, a band corresponding to N1-BR18 with the three glycan site mutations (NHG 3Q) was not observed, indicating the HA to NA ratio increased (Fig. 5B). Although the N1-BR18 NHG (3Q) mutant was not visible by Coomassie staining, the virus displayed NA activity levels of ~20% of the WT when

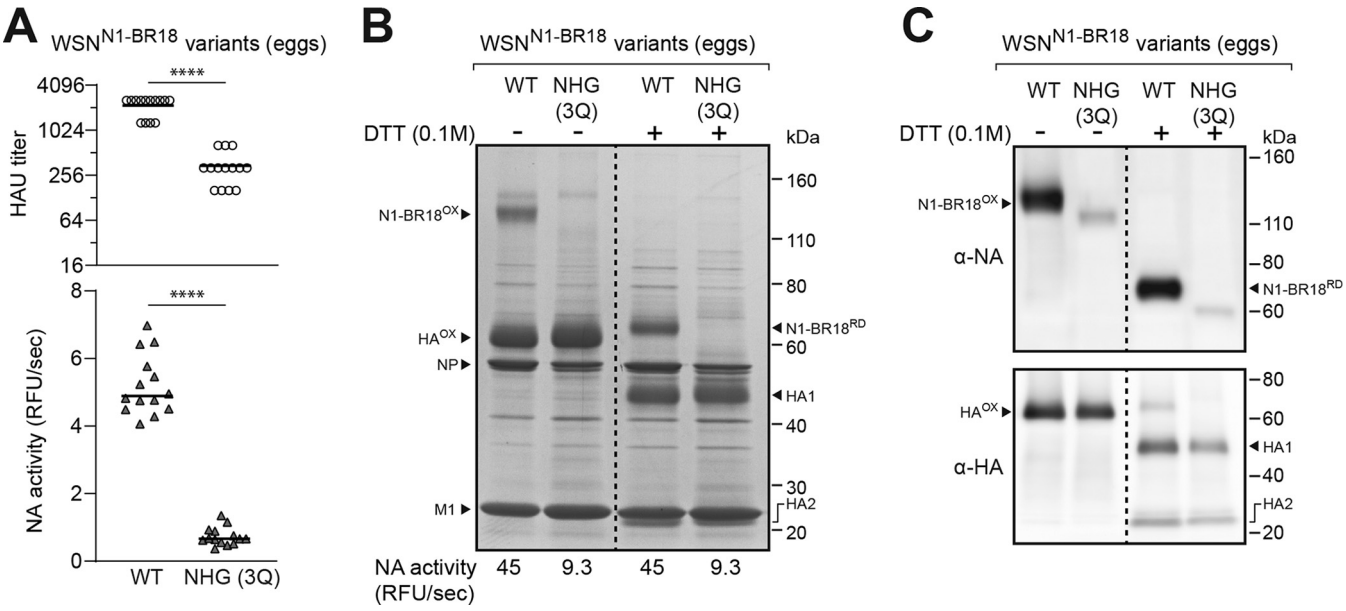

FIG 5 N1 viral incorporation is reduced when the conserved head glycosylation sites are absent. (A) Scatterplots of the HAU titers and NA activities in the allantoic fluid harvested from eggs infected with recombinant WSN viruses carrying N1-BR18 (WT) or N1-BR18 with no head glycan sites (NHG 3Q), which was generated by Gln mutations of each head glycosylation site (N88Q, N146Q, and N235Q). The viruses were rescued by reverse genetics and passaged twice in eggs. The data points from individual eggs following the second passage are shown with the median. *P* values (95% CI) are from a two-tailed unpaired *t* test. (B) Representative image of a Coomassie-stained SDS-PAGE gel containing the indicated recombinant WSN$^{N1\text{-}BR18}$ viruses. The allantoic fluid from a second passage in eggs was pooled, the virions were isolated by centrifugation, and the protein concentration was determined. Samples containing ~5 μg of total protein were treated with the reductant DTT as indicated and resolved using a 4–12% Tris-glycine SDS-PAGE gel. Intermolecular (N1-BR18^{OX}) and intramolecular (HA^{OX}) disulfide-bonded NA and HA are indicated along with the reduced forms (N1-BR18RD, HA1, and HA2). The viral proteins NP and M1 are also indicated. The NA activity listed below the gel was measured using equal total protein amounts of the two viruses. (C) NA and HA immunoblots of the isolated recombinant WSN$^{N1\text{-}BR18}$ viruses. Samples containing equal total protein amounts were treated with DTT as indicated, resolved using a 4%–12% Tris-glycine SDS-PAGE gel, and transferred to a PVDF membrane prior to immunoblotting.

equal viral protein amounts were analyzed (Fig. 5B), and the protein was also detected as a less intense, faster-migrating band by immunoblotting, confirming its presence in virions at lower levels (Fig. 5C).

To examine how the observed defects impact virus replication, WSN and PR8 viruses carrying N1-BR18 WT and the NHG 3Q mutant were passaged twice in eggs, and the 50% egg infective dose (EID_{50}) as well as the median tissue culture infectious dose ($TCID_{50}$) were measured (Table 1). For each virus, the EID_{50} value was higher than the $TCID_{50}$ value. In line with the HAU titers, the N1-BR18 NHG 3Q mutant in the PR8 and the WSN backbone reached lower titers than the respective WT in eggs and cells. Together, these results demonstrate that infectious H1N1 viral production and NA incorporation both decrease when the three conserved glycosylation sites on the N1 head domain are absent.

The variable glycosylation sites in the N1 head domain from human H1N1 IAVs. Previous studies have demonstrated that the N-linked glycosylation sequence N-X-T is more efficiently recognized than N-X-S (44). Based on sequence alignments of the human N1 head domain, three of the main variable glycosylation sites (Asn365,

TABLE 1 Infectious viral titers determined using eggs and MDCK cells

Viral backbone	NA	EID_{50}/ml	$TCID_{50}$/ml
PR8	N1-BR18 (WT)	1.47×10^{10}	1.78×10^{6}
PR8	N1-BR18 NHG (3Q)	3.16×10^{9}	7.5×10^{4}
WSN	N1-BR18 (WT)	6.81×10^{9}	1.33×10^{7}
WSN	N1-BR18 NHG (3Q)	3.16×10^{8}	3.16×10^{6}
WSN	N2-KA17 (WT)	6.81×10^{8}	3.16×10^{7}
WSN	N2-KA17 CHG (2Q)	3.16×10^{8}	2.37×10^{6}
WSN	N2-KA17 VHG (4Q)	1.47×10^{9}	1.78×10^{7}
WSN	N2-KA17 NHG (6Q)	6.81×10^{7}	7.50×10^{5}

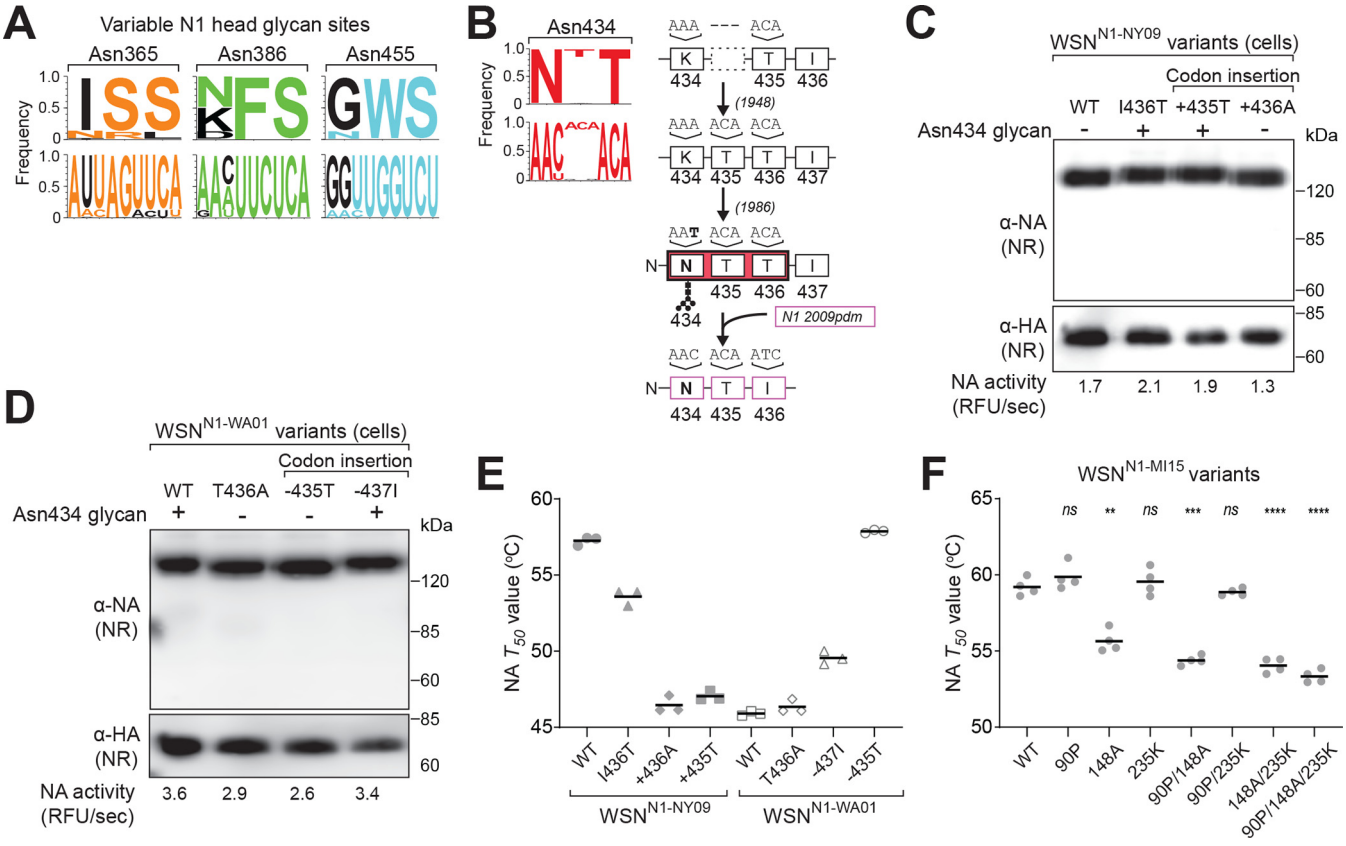

FIG 6 N1 stability decreases from the head domain insertion that creates the variable Asn434 glycosylation site. (A) Logo plots displaying the amino acid (top) and nucleotide (bottom) frequency for the three N-X-S variable glycosylation sites on the N1 head domain from human H1N1 IAVs. (B) Amino acid (top) and nucleotide (bottom) logo plot for the N-X-T variable glycosylation site in the N1 head domain from human H1N1 IAVs. A timeline showing when the insertion and the necessary mutations appeared in the database is included to the right. Note that the N1 insertion was lost in 2009 when the pandemic H1N1 IAV of swine origin became prevalent. (C and D) Representative NA and HA immunoblots of recombinant WSN viruses carrying N1-NY09 with the indicated mutations and insertions (C) or N1-WA01 with the indicated mutations and deletions (D). The viruses were rescued by reverse genetics and passaged in MDCK cells, and the virus-containing supernatants were sedimented, resuspended in equal volumes, and resolved by NR SDS-PAGE. (E) NA T_{50} values (the temperature at which 50% of NA activity remains) are displayed for the recombinant WSN viruses carrying N1-NY09 or N1-WA01 with the indicated mutations, insertions, or deletions. The measurements ($n = 3$ biologically independent experiments) were taken in tissue culture medium with the NA activity at 37°C set to 100%. The line represents the means. (F) NA T_{50} temperatures are displayed for the WSN reassortant viruses carrying N1-MI15 with the indicated glycan site mutations. The measurements ($n = 4$ biologically independent experiments) were taken in tissue culture medium with the NA activity at 37°C set to 100%. The line depicts the means, and the *P* values (95% CI) were determined with respect to the WT by one-way ANOVA.

Asn386, and Asn455) use N-X-S, and these sites likely change by substitutions at either the N or S residues (Fig. 6A). In contrast, the other variable glycosylation site (Asn434) uses N-X-T and appears to have been created by a T codon insertion combined with an N substitution that occurred later (Fig. 6B). The codon insertion is almost exclusively found in human H1N1 IAVs beginning in 1948 and ending when the 2009 pandemic H1N1 virus, which carries a N1 gene segment of swine origin, was introduced to the human population (Fig. 6B). Positionally, the Asn434 site is located near the conserved Asn146 site, and out of the seven most prevalent glycosylation sites, these are the only two with the more efficient recognition sequence, suggesting they impact N1 more than the others.

To investigate this site, two similar natural sequences were identified that lack or have the insertion resulting in the Asn434 glycosylation site. Several mutations were then introduced into the NA lacking the insertion (N1-NY09), which is from a 2009 pandemic-like H1N1 strain (A/New York/18/2009), and an NA possessing the insertion (N1-WA01), which is from a 2001 seasonal H1N1 strain (A/Waikato/7/2001). For N1-NY09, these involved creating a glycosylation site by mutation (I436T) and codon insertion (+435T) and a control where a codon insertion (+436A) was made that does not create a glycosylation site. All the mutants were rescued using a WSN backbone

and propagated using MDCK cells, where no growth defect was observed based on cytopathic effects. Activity measurements and immunoblot analysis of the isolated particles showed no significant change in the N1-NY09 levels, and the mutants with the additional glycosylation site (I436T and +435T) displayed the expected mobility increase (Fig. 6C). Similar results were obtained from viruses carrying N1-WA01 with converse mutations that removed the glycosylation site (T436A), the codon insertion responsible for the glycosylation site (−435T), or a downstream codon (−437I) that left the site (Fig. 6D).

As Asn434 is near the central Ca^{2+} binding site, which is a major determinant for NA stability (26), we asked if this glycan influences NA thermostability. For N1-NY09, introducing the insertion and the glycosylation site (+435T) caused the thermostability to drop to a level that almost matched N1-WA01. Conversely, deleting this codon (−435T) in N1-WA01 increased the thermostability to the level of N1-NY09 (Fig. 6E). However, the analysis of the other mutants indicated that the stability changes are more associated with the insertion (+436A) for N1-NY09 and deletion (−437I) for N1-WA01 than the glycan addition or removal (Fig. 6E). This implies that structural changes imparted by the codon insertion or deletion affect N1 stability by altering the oligomeric assembly that creates the central Ca^{2+} binding site. We then tested this more broadly by examining the conserved head glycan site mutants. Interestingly, all N1-MI15 mutants lacking the N-X-T site at Asn146 (148A) possess decreased thermostability, indicating that both N-X-T head glycosylation sites contribute to N1 thermostability (Fig. 6F).

Analysis of N-linked glycan sites encoded by the NA from H3N2 IAVs. H3N2 IAVs commonly circulate together with H1N1 IAVs in the human population. Therefore, we also analyzed the subtype 2 (N2) sequences from H3N2 IAVs. In contrast to N1, the avian, swine, and human N2 sequences all vary in the number of predicted N-linked glycosylation sites, with swine N2s having the most, followed by the human and avian N2s (Fig. 7A, left). Surprisingly, almost all N2 sequences were found to contain two sites in the stalk (Fig. 7A, middle), resulting in the head domain being responsible for the variation in the number of N2 glycosylation sites (Fig. 7A, right).

Positional analysis showed that four of the N-linked glycosylation sites are highly conserved in the N2s and that many variable sites are biased toward the species of origin of the strain (Fig. 7B). Of the four conserved sites, three (Asn86, Asn146, and Asn234) are nearly identical to N1, and the fourth (Asn200) is located on the side near the dimer interface. In contrast to N1, N-X-T is the most prevalent glycosylation sequence in the N2 head, as it is used for three of the conserved sites and three of the common variable sites (Fig. 7B). The temporal analysis showed that most avian N2s carry five sites, whereas the swine and human N2 head domains increased from five to six and seven sites in more recent H3N2 isolates (Fig. 7C). These observations suggest that N2s require more head domain glycans for folding, can accommodate more glycans on the head domain, and/or that the N2 head domain is under more selection pressure than N1.

Contributions of the N2 head glycan sites to viral replication, incorporation, and stability. To examine the functional contributions of the N2 head glycosylation sites, several mutants were created using an NA (N2-KA17) from a recently recommended H3N2 vaccine strain (A/Kansas/14/2017) and rescued with a WSN backbone. Following passaging in eggs, lower HAU titers and NA activity levels were obtained for the N2-KA17 mutant viruses that contain only the four conserved head glycosylation sites (CHG 2Q) or the two variable glycosylation sites (VHG 4Q) at Asn245 and Asn367, and these values decreased further for the N2-KA17 mutant virus with no head glycosylation site (NHG 6Q) (Fig. 7D). Upon analysis of the isolated virions, oxidized N2-KA17 dimers were readily apparent for WT that can be reduced by DTT (Fig. 7E). Similar faster-migrating bands were observed for the CHG 2Q and VHG 4Q mutants, but the band corresponding to the NHG 6Q mutant was faint. In line with these results, the viruses carrying the CHG 2Q and VHG 4Q mutants possessed ~50% of the NA activity

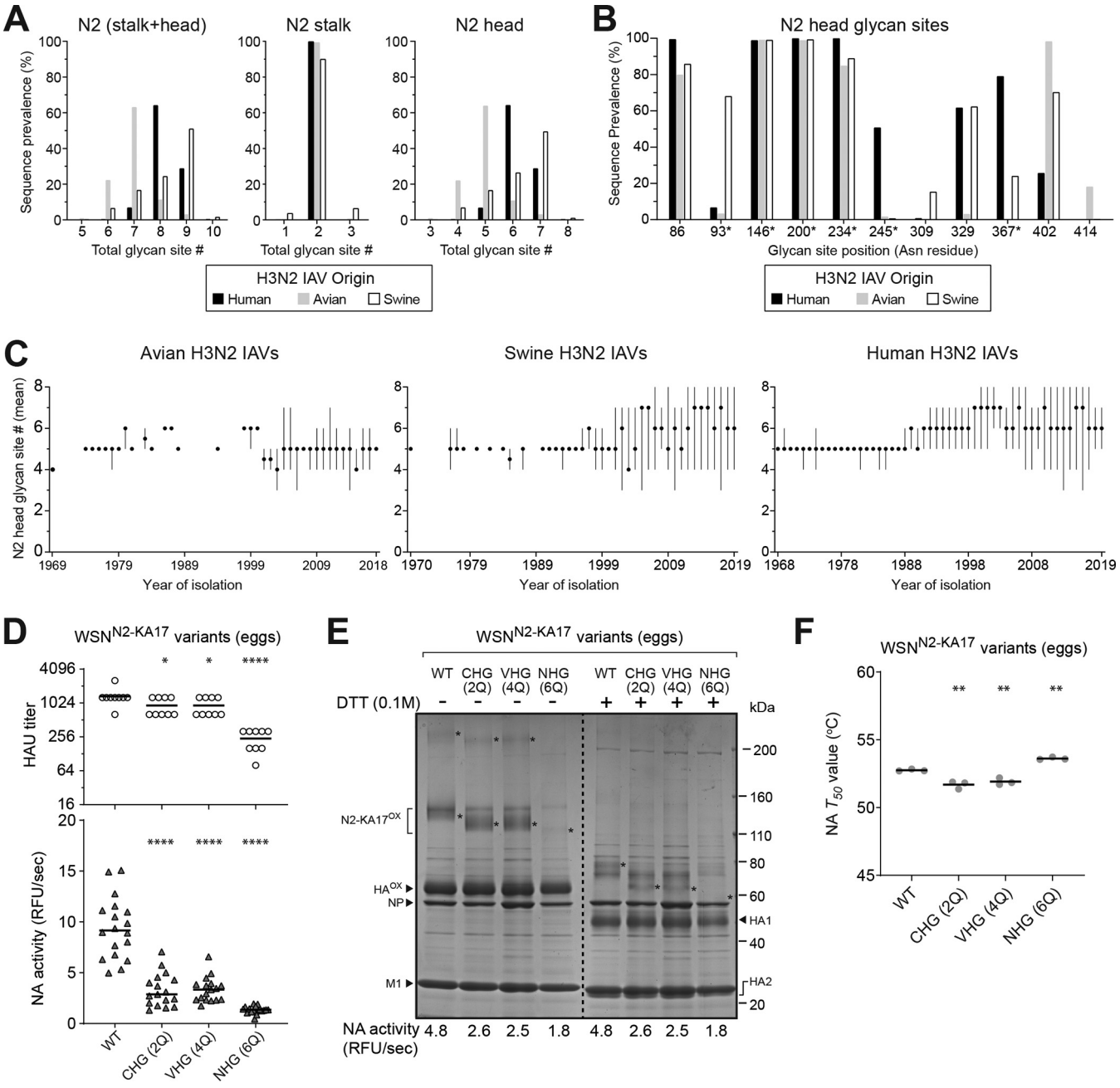

FIG 7 Analysis of the NA glycan sites from H3N2 IAVs. (A) Graphs showing the prevalence of NA sequences from human ($n = 24,184$), swine ($n = 3,484$), and avian ($n = 411$) H3N2 IAVs that possess the indicated number of glycosylation sites in the stalk and head domain (left), the stalk alone (middle), and the head domain alone (right). (B) Prevalence of the most frequent glycosylation sites in the N2 head domain sequences is shown based on the H3N2 IAV strain species origin. The glycan site position refers to the Asn (N) in the N-X-S/T sequence. Sites with an N-X-T sequence have an asterisk. (C) Graphs displaying the mean number of glycosylation sites in the N2 head domain with respect to the year the avian (left), swine (middle), and human (right) H3N2 IAVs were isolated. Filled circles correspond to the means, and lines show the range in the site number for the sequence sets from each year. Sequences were obtained from the NCBI Influenza Database. (D) Scatterplot of the HAU titers and NA activities from the allantoic fluid of individual eggs infected with recombinant WSN viruses carrying N2-KA17 (WT) or mutants that contain only the conserved head glycan sites (CHG 2Q), variable head glycan sites (VHG 4Q), or no head glycan sites (NHG 6Q). Data from the second passage are shown with the medians. *P* values (95% CI) were determined with respect to the WT by a one-way ANOVA. (E) The recombinant WSN$^{N2\text{-}KA17}$ viruses were isolated from allantoic fluid by centrifugation, separated by SDS-PAGE, and visualized by Coomassie staining. Prior to loading, ~5 μg of total protein was treated with DTT or left untreated. The NA activity for each virus was measured using equal protein amounts. Asterisks mark bands corresponding to N2-KA17 dimers and tetramers (−DTT) or reduced monomers (+DTT). (F) NA T_{50} temperatures were determined for the indicated WSN reassortant viruses in PBS, pH 7.2, with 1 mM $CaCl_2$. NA activity at 37°C was set to 100%. The line is the means, and the *P* values (95% CI) were calculated with respect to the WT by one-way ANOVA.

levels found in the virus containing N2-KA17 WT, whereas the NHG 6Q mutant virus possessed ~35% (Fig. 7E). Consistent with these results, the virus carrying the N2-KA17 NHG (6Q) mutant registered lower titers in eggs and cells than the viruses carrying N2-KA17 WT, the CHG (2Q) mutant, or the VHG (4Q) mutant (Table 1), supporting the notion that N-linked glycans on the NA head domain are needed for optimal replication. Based on the relatively high retention of N2 when the head glycan sites were absent, we also examined the stability of the N2 mutants. In contrast to N1, the thermostability of N2 did not significantly change upon removal of the head glycans (Fig. 7F), indicating that N-linked glycan addition and removal has a limited structural impact on N2.

DISCUSSION

In this study, sequence-based analyses were combined with several experimental approaches to examine the potential functions of the N-linked glycans on NA from H1N1 and H3N2 IAVs. Our results show that three glycosylation sites (Asn88, Asn146, and Asn235) are well conserved on the N1 head domain and that N2 possesses four conserved sites (Asn86, Asn146, Asn200, and Asn234), three of which are similar in position. Based on the available sequences, it appears that the variable glycosylation sites on the NA head domain are primarily found on human H1N1 IAV strains and that nucleotide substitutions, insertions, and/or deletions are likely responsible for the temporal nature of these sites, together with reassortant events that involve the NA gene segment, such as the introduction of the 2009 pandemic H1N1 virus of Eurasian swine origin (40–42). In contrast, the variable sites on the NA head domain in H3N2 strains are not exclusive to the species of origin and mainly appear to result from nucleotide substitutions.

Despite the positional conservation, none of the head domain glycosylation sites were observed to be essential for viral replication in MDCK cells or eggs, indicating IAVs are not significantly impacted if a particular site is inefficiently recognized. In line with a potential role in NA maturation (21), viral growth showed an impairment when all the conserved sites on the NA head domain were absent and the defect coincided with a decrease in the virion incorporation of NA. However, NA activity was detected in all the viruses containing mutations in the head glycosylation sites, indicating some portion of NA can properly mature when one or more of the conserved head domain sites are absent, raising the question of why these sites are conserved in nature.

Previous work has shown that efficient IAV replication is dependent on a balance between the receptor-binding function of HA with the receptor-destroying function of NA (46–49). This implies that the viral growth defects we observed with the mutants lacking the NA head domain glycosylation sites likely result from a disruption of the NA and HA balance due to the lower NA amounts in the virion. Therefore, we suspect that if these mutant viruses were passaged further, replication could be improved by reversions in NA or mutations in HA that restore the balance by altering the receptor binding pocket, similar to previous results for NA-deficient virions (46–48). Whether potential rescue mutations would occur faster in eggs or MDCK cells is not entirely clear. Ultimately, it may depend on several factors in addition to changes in the replication environment, temperature, and exogenous protease addition, as our titer measurements suggest the growth defect is more pronounced in cells with a PR8 backbone and eggs with a WSN backbone.

Although the study primarily focused on H1N1 and H3N2 IAVs, we also found that the conserved glycosylation sites on the N1 head domain (Asn88, Asn146, and Asn235) are highly prevalent in avian and swine IAV strains carrying an H*x*N1 subtype combination, where *x* is any of the other 16 HA subtypes. The conserved sites in the N2 head domain (Asn86, Asn146, Asn200, and Asn234) also exist at a high frequency in human H2N2 strains and swine and avian H*x*N2 strains, but in the latter two, lower conservation was observed for the Asn86 and Asn234 sites. Interestingly, only the Asn146 site is conserved in all other avian NA subtypes (note that it varies from position 143 to 148 in N3 to N9), and the highly prevalent sites in the head domains of these subtypes vary

in number from two to five, as well as position, indicating the function of NA head glycans differs between subtypes.

Inefficient recognition of the glycosylation sites may be one reason why multiple sites are conserved, as growth defects were only clear when multiple conserved glycan sites were absent. Along these lines, some H1N1 strains that lack one of the three conserved head glycosylation sites have been found, and only the Asn146 site is the more efficiently recognized sequence N-X-T in H1N1 IAVs, and it is also present in all other NA subtypes at or near this position (44). However, three of the conserved N2 head domain sites contain the N-X-T sequence (Asn146, Asn200, and Asn234), and the gel shifts that were observed indicate the different sites are generally recognized. These observations suggest that the individual sites could provide a subtle increase in the replication efficiency of H1N1 IAVs that was not detected by our assays, but it is equally plausible that the conserved sites provide a growth or immunogenicity advantage *in vivo*, which has been reported for several other viral glycoproteins (50–52).

Supporting a possible role *in vivo*, the two N-X-T sites on the N1 head domain (Asn146 and Asn434) both affected the enzymatic properties, and the conserved site at Asn146 has previously been reported to possess a unique, wide array of branched glycan structures (36). The sites are also proximal to one another and near the central Ca^{2+} binding site on top of the N1 tetramer, indicating the glycan or the site alters the conformation-dependent affinity for this Ca^{2+}, which is a major NA stability determinant (26). Along these lines, less significant stability effects were observed when the variable N-X-T site was inserted into an N1 (NA/CA09) with a lower central Ca^{2+} binding site affinity (data not shown). Currently, we cannot investigate the structural consequence of the insertion more directly because structures do not exist for a human N1 head domain between 1948 and 2009, which contains the amino acid insertion resulting in the additional glycosylation site.

An interesting observation is that N1 sequences predominantly utilize the N-X-S consensus glycosylation site, whereas N2 sequences are significantly biased toward N-X-T sites and some sites show species specific X residues. This suggests that the conserved N1 site is required for a specific function, such as limiting epitope access. However, an enzyme-linked lectin (ELLA) analysis (53) of viruses containing N1-NY09 with and without the insertion and Asn434 glycan addition showed no difference in reactivity to a ferret antiserum raised against an NA (N1-CA09) that is almost identical in sequence to N1-NY09 (data not shown). Conversely, N1-WA01 did not gain reactivity against the same antiserum when the deletion was introduced (data not shown), indicating that the antigenic changes between these two strains is not related to the removal or addition of the Asn434 glycosylation site in the human N1 head domain. While this was somewhat surprising, the region surrounding the central Ca^{2+}-binding site on the N1 tetramer has been shown to be highly conserved (26), indicating this region is not subject to significant selection pressure or that antibody binding to this region does not negatively impact viral replication.

Assigning functions to N-linked glycans on viral glycoproteins is difficult, as a role in maturation does not exclude an additional role in altering surface epitopes. The observation that the number of glycan sites on the N1 head domain have both increased and decreased over time, whereas those on N2 have primarily increased in number, suggests that glycan site addition has subtype-dependent effects. Supporting this possibility, N2 has a higher prevalence of head glycosylation sites and variable sites, and the N1 variable site at Asn386, which was introduced during the 2009 pandemic, was quickly lost in the circulating strains, something that is a bit perplexing, since N1 variants carrying four sites appear less common in swine H1N1 IAVs than those carrying three. There also are additional glycosylation sites with a low frequency in the database that we did not examine, indicating some will be advantageous in specific populations. The results in this study demonstrate that the glycosylation sites on the NA head domain are required for efficient virion incorporation and replication, indicating mutations in these sites are useful for creating attenuated IAV strains. Conversely, changing the glycosylation site recognition sequence or adding variable sites may improve

NA folding and, hence, virion incorporation, which could be utilized to produce vaccine strains that possess a higher NA to HA ratio. By combining these different mutation approaches, it should be possible to further define how the N-linked glycan sites on NA contribute to IAV viability, antigenicity, antibody binding, and transmissibility, in addition to their likely function during maturation.

MATERIALS AND METHODS

Reagents and antibodies. Dulbecco's modified Eagles medium (DMEM), fetal bovine serum (FBS), L-glutamine, penicillin-streptomycin (P/S), Opti-MEM (OMEM), anti-goat IgG horseradish peroxidase (HRP)-linked secondary antibody, simple blue stain, Novex 4%–12% Tris-glycine SDS-PAGE gels, Lipofectamine, and dithiothreitol (DTT) were all purchased from Thermo Fisher Scientific. 2′-(4-methylumbelliferyl)-α-D-*N*-acetylneuraminic acid (MUNANA) was obtained from Cayman Chemical. Anti-rabbit IgG HRP-linked secondary antibody and 0.45-μm polyvinylidene difluoride (PVDF) membrane were obtained from GE Healthcare. Specific-pathogen-free (SPF) eggs and turkey red blood cells (TRBCs) were purchased from Charles River Labs and the Poultry Diagnostic and Research Center (Athens, GA), respectively. Rabbit antiserum against NA was generated by Agrisera (Sweden) using NA-WSN33 residues 35 to 453, isolated from *Escherichia coli* inclusion bodies. Polyclonal goat antisera against influenza virus HAs from A/California/04/2009 (NR-15696) and A/Fort Monmout/1/1947 (NR-3117) both were obtained from BEI Resources, NIAID, NIH.

Plasmids and constructs. The eight reverse genetics (RG) plasmids carrying the PR8 and WSN33 gene segments were provided by Robert Webster (St. Jude Children's Research Hospital). The RG plasmid containing NA (N1-NY09) from the H1N1 strain A/New York/18/2009 was described previously (26). The NA gene segments from the strains A/Waikato/7/2001 (N1-WA01), A/Michigan/45/2015 (N1-MI15), and A/Kansas/14/2017 (N2-KA17) and the CHG 2Q, VHG 4Q, and NHG 6Q mutants were all synthesized (Eurofins Genomics or GenScript) and used to generate the RG plasmids as follows. The pHW2000 plasmid backbone (54) and the NA gene segments were amplified by PCR using forward and reverse primers (Table 2) with complementary NA 5′ and 3′ untranslated region overhangs that direct the recombination upon transformation into *E. coli* (55). The N1-BR18 RG plasmid was generated by cloning the NA gene segment from the H1N1 strain A/Brisbane/02/2018 IVR-190, grown in SPF eggs, into the plasmid pHW2000 following PCR amplification (56). Mutations in the N1-MI15 head domain (S90A, S90P, T148A, and line N235K) and the N1-BR18 head domain (N86Q, N146Q, and N235), codon insertions in N1-NY09 (+435T and +436A), codon deletions in N1-WA01 (−435T and −437I), and the substitutions in N1-NY09 (I436T) and N1-WA01 (T436A) all were made with site-directed mutagenesis primers (Table 3) using the respective NA RG plasmid as a template. All constructs were confirmed by sequencing (Eurofins MWG Operon or the FDA core facility).

Cell culture and viral reverse genetics. Madin-Darby canine kidney 2 (MDCK.2; CRL-2936) cells and HEK 293T/17 cells (CRL-11268), obtained from LGC Standards, were cultured in DMEM containing 10% FBS and 100 U/ml P/S in a 37°C atmosphere with 5% CO_2 and ~95% humidity. Reassortant viruses carrying N1-MI15, N1-NY09, or N1WA01 variants were generated by 8-plasmid reverse genetics using the indicated NA and the complementary seven backbone gene segments of WSN33 as previously described (26). Reassortant viruses carrying N1-BR18 or N2-KA17 variants were generated by 8-plasmid reverse genetics using the seven backbone gene segments of WSN33 or PR8, as follows, using 6-well plates. One day before the experiment, 1.2×10^6 293T cells and 1.2×10^6 MDCK.2 cells were plated per well using 3 ml DMEM with 10% FBS. The next day, the medium was replaced with 2 ml of OMEM, the eight plasmids were added to 200 μl of OMEM at a concentration of 1 μg per plasmid and combined with 18 μl of Lipofectamine, and the mixture was incubated for 45 min at room temperature. The cell medium was removed, the mixture was added to one well, and the dish was incubated 5 min at 37°C before 800 μl OMEM was added to each well. Approximately 24 h posttransfection, 1 ml OMEM containing 4 μg/ml tosylsulfonyl phenylalanyl chloromethyl ketone (TPCK) trypsin was added to each well. Culture medium was harvested between 72 and 96 h posttransfection, clarified by centrifugation (2,000 × *g*; 5 min), and passaged using SPF eggs or MDCK.2 cells.

Viral passaging in MDCK.2 cells and SPF eggs. For cell passaging, 1 day after seeding 1×10^6 MDCK.2 cells on a 6-cm dish, the culture medium was removed and the cells were washed with 1 ml infection medium (IM) comprised of DMEM, 0.3% BSA, 0.1% FBS, and P/S. Each dish then received 2 ml of cold IM containing 10 μl of the clarified viral reverse genetics medium and was rocked at 4°C for 30 min. The inoculation medium was then removed, cells were washed with 1 ml of IM, 5 ml of IM containing 10 μg/ml TPCK-trypsin was added, and the dish was placed at 37°C. The culture medium was harvested at the peak of cytopathic effects (~48 to 72 h postinfection) and clarified by centrifugation (2,000 × *g*; 5 min) prior to analysis, storage, or sedimentation. Passaging in SPF eggs was carried out by inoculating 100 μl of clarified viral reverse genetics medium into 9- to 11-day-old embryonated eggs and incubating them for 3 days at 33°C. Following the incubation, eggs were chilled at 4°C for 2 h, and the allantoic fluid from each egg was harvested, clarified by centrifugation (2,000 × *g*; 5 min), and stored in aliquots at −80°C. Viruses in the allantoic fluid from the first passage were then diluted (1:1,000) in sterile phosphate-buffered saline (PBS), and 100 μl was used to inoculate the 9- to 11-day-old embryonic eggs. For each virus, groups of eight or seven eggs were used, and the allantoic fluid from each egg was harvested individually and clarified by centrifugation (2,000 × *g*; 5 min) prior to analysis or sedimentation.

Viral sedimentation and sucrose gradient isolation. Clarified virus-containing culture medium (~8 ml) or allantoic fluid (~28 ml) was added to ultracentrifuge tubes, and a sucrose cushion (25%,

TABLE 2 Primers for inserting the NA gene segments into the pHW2000 plasmid

NA or plasmid	Forward primer, 5′ to 3′	Reverse primer, 5′ to 3′
N1-WA01	GAAGTTGGGGGGGAGCAAAAGCAGGAGTTTAAAATGAATC	GGTTATTAGTAGAAACAAGGAGTTTTTTCAACGGAC
N1-MI15	CGACCTCCGAAGTTGGGGGGAGCAAAAGCAGGAGTTTAAAATGAATC	CATTTTGGGCCGCCGGGTTATTAGTAGAAACAAGGAGTTTTTTGAAC
N1-BR18	TATTCGTCTCAGGGAGCAAAAGCAGGAGT	ATATCGTCTCGTATTAGTAGAAACAAGGAGTTTTTT
N2-KA17	CGACCTCCGAAGTTGGGGGGGAGCAAAAGCAGGAGTG	CATTTTGGGCCGCCGGGTTATTAGTAGAAACAAGGAG
pHW2000	CCTTGTTTCTACTAATAACC	CCTGCTTTTGCTCC

wt/vol, sucrose, PBS, pH 7.2 and 1 mM $CaCl_2$) equal to ~15% of the sample volume was layered under each sample. Virions were then isolated by sedimentation (100,000 × *g*; 45 min) at 4°C and the supernatant was aspirated. Cell-produced viral pellets were resuspended in 200 μl PBS, pH 7.4, and 1 mM $CaCl_2$, and NA activity was analyzed prior to immunoblotting. Egg produced virions were resuspended in 200 μl of PBS, pH 7.2, containing 1 mM $CaCl_2$. For sucrose gradient isolations, the resuspension solution containing 12.5% (wt/vol) sucrose was layered on top of a discontinuous gradient containing four 8.5-ml sucrose layers (60%, wt/vol, 45%, wt/vol, 30%, wt/vol, and 15%, wt/vol, sucrose in PBS, pH 7.2, and 1 mM $CaCl_2$) and centrifuged at 100,000 × *g* for 2 h at 4°C. Fractions were isolated from top to bottom, the density was determined with a refractometer, and those corresponding to 30% to 50% (wt/vol) sucrose were pooled and mixed with 2 volumes of PBS, pH 7.2, and 1 mM $CaCl_2$, and the virions were sedimented (100,000 × *g*; 45 min). The supernatant was discarded, and the viral pellet was resuspended in 250 μl PBS, pH 7.2, containing 1 mM $CaCl_2$. Total protein concentrations in resuspended viral pellets all were determined with a bicinchoninic acid protein assay kit (Pierce) using the 96-well plate protocol. The average value was determined from the 1:2 and 1:4 sample dilutions, and each sample was adjusted to a final concentration of 1 mg/ml using PBS, pH 7.2, containing 1 mM $CaCl_2$.

HAU titer, NA activity, and thermostability measurements. HAU titers were determined using a 96-well plate and 0.5% TRBCs in PBS, pH 7.2. Briefly, 90 μl of PBS, pH 7.2, was added to the first column and 50 μl to remaining columns. From each infected egg, 10 μl of allantoic fluid was added to the first column, creating a 1:10 dilution. A 2-fold serial dilution was made by transferring 50 μl from each column to the subsequent column, and 50 μl of 0.5% TRBCs was added to each well. The plate was incubated for 30 min at room temperature, and the HAU titer was determined as the last well where agglutination was observed. For sialidase activity measurements, equal amounts of clarified virus-containing medium, allantoic fluid, or sedimented viral samples were brought up to 195 μl in reaction buffer (0.1 M KH_2PO_4, pH 6.0, and 1 mM $CaCl_2$), transferred to a 96-well black clear-bottom plate (Corning), and incubated at 37°C for 15 min. Reactions were then initiated by adding 5 μl of 2 mM MUNANA and the fluorescence was measured with either a SpectraMax Gemini EM plate reader or a Cytation 5 (Biotek) using 365-nm excitation and 450-nm emission wavelengths. NA thermostability was determined by exposing equal amounts of clarified virus-containing media to temperatures ranging from 37°C to 64°C for 10 min and measuring the residual sialidase activity as previously described (26).

EID_{50} and $TCID_{50}$ measurements. Each virus was generated by reverse genetics and passaged twice in 9- to 11-day-old SPF embryonated eggs. The allantoic fluid from the second passage was harvested, clarified by centrifugation (2,000 × *g*; 5 min), and used to create 1:10 serial dilutions in sterile PBS. To determine the EID_{50}, each dilution between 10^{-5} and 10^{-11} was used to inoculate three eggs. Each 100-μl inoculum was delivered by separate 27-gauge needles attached to 1-ml syringes, and the eggs were incubated at 33°C for 3 days. The allantoic fluid from each egg was harvested and clarified (2000 × *g*; 5 min), and the infected eggs were identified based on the presence of NA activity and positive HAU titers. The $TCID_{50}$ value for each virus was determined the same day using the same 1:10 dilution series to infect confluent MDCK.2 cells on a 96-well plate. First, the plate was washed with cold IM, after which each column (eight wells) were infected with a corresponding viral dilution, ranging from 10^{-1} to 10^{-11}, using a 100-μl inoculum for each well. The plate was incubated at 4°C for 30 min to allow

TABLE 3 Primers for introducing site-directed mutations in the NA head domain

NA	Mutation	Forward primer, 5′ to 3′	Reverse primer, 5′ to 3′
N1-MI15	S90A	GCAATTCCGCTCTCTGCCCTG	CAGGGCAGAGAGCGGAATTGC
N1-MI15	S90P	GCAATTCCCCTCTCTGCCCTG	CAGGGCAGAGAGGGGAATTGC
N1-MI15	T148A	CATTCCAATGGAGCCATTAAAGACAGG	CCTGTCTTTAATGGCTCCATTGGAATG
N1-MI15	N235K	GTGCATGTGTAAAAGGTTCTTGCTTTACC	GGTAAAGCAAGAACCTTTTACACATGCAC
N1-BR18	N88Q	CGTGAAATTAGCGGGCCAGTCCTCTCTCTGCCCTG	CAGGGCAGAGAGAGGACTGGCCCGCTAATTTCACG
N1-BR18	N146Q	TTGCTAAATGACAAACATTCCCAGGGAACCATTAAAGACAGGAGC	GCTCCTGTCTTTAATGGTTCCCTGGGAATGTTTGTCATTTAGCAA
N1-BR18	N235Q	GAGTCTGAATGTGCATGTGTACAGGGTTCTTGCTTTACCATAATG	CATTATGGTAAAGCAAGAACCCTGTACACATGCACATTCAGACTC
N1-NY09	I436T	GAGAACACAACCTGGACTAGCGGGAGCAG	GCTAGTCCAGGTTGTGTTCTCTTTGGGTCG
N1-NY09	+435T	AAAGAGAACACAACAATCTGGACTAGCGGGAGC	CCAGATTGTTGTGTTCTCTTTGGGTCGCCCTC
N1-NY09	+436A	GAGAACACAGCTATCTGGACTAGCGGGAGC	AGTCCAGATAGCTGTGTTCTCTTTGGGTCGC
N1-WA01	T436A	AGAAAATACAGCAATCTGGACTAGTGGGAGC	TCCAGATTGCTGTATTTTCTTTTGGCAGTCC
N1-WA01	−435T	AAAAGAAAATACAATCTGGACTAGTGG	TCCAGATTGTATTTTCTTTTGGCAGTCC
N1-WA01	−437I	AGAAAATACAACATGGACTAGTGGGAGCAGC	TAGTCCATGTTGTATTTTCTTTTGGCAGTCC

for viral attachment, after which the inoculum was removed, and the wells were washed with 100 μl IM prior to adding 100 μl of fresh 37°C IM containing 4 μg/ml TPCK-trypsin to each well. The plate was then placed in a humidified incubator at 37°C, and the infected wells were determined based on cytopathic effects at 72 h. Final EID_{50} and $TCID_{50}$ values per milliliter were determined as previously described (57).

SDS-PAGE, Coomassie staining, and immunoblotting. Sedimented viral samples containing equal resuspension volumes or the indicated total protein amounts were mixed with Laemmli sample buffer that contained 0.1 M DTT, as indicated. Samples were then heated at 37°C or 50°C for 10 min and resolved by either 7.5% (α-NA), 11% (α-HA), or 4% to 12% (α-NA, α-HA, and Coomassie) Tris-glycine SDS-PAGE gels. Gels were Coomassie stained using simple blue or transferred to a 0.45-μm-pore PVDF membrane at 15 V for 1 h. PVDF membranes were blocked with milk-PBST (3% nonfat dry milk, PBS, pH 7.4, 0.1% Tween 20) for 30 min and processed using standard immunoblotting protocols with the indicated antibodies and the appropriate HRP-linked secondary antibody. Immunoblots were developed with the SuperSignal West Femto kit (ThermoFisher) and imaged using an Azure C600 or a Syngene G Box.

Analysis of NA glycosylation sites and *in silico* glycosylation models. Complete NA protein sequences from H1N1 and H3N2 IAVs of human, avian, and swine origin were downloaded from The Influenza Virus Resource at the National Center for Biotechnology Information (58). Each group was aligned using MAFFT v7.311 with the default progressive method (FFT-NS-2). Mislabeled sequences were manually removed. The final NA data sets consist of 18,966 sequences from human H1N1 strains (1918-2019/11/20), 630 sequences from avian H1N1 strains (1976-2018/11/16), 4,949 sequences from swine H1N1 strains (1930-2019/12/20), 24,184 sequences from human H3N2 strains (1968-2019/11/09), 411 sequences from avian H3N2 strains (1969-2018/10/13), and 3,484 sequences from swine H3N2 strains (1970-2019/12/19). Potential glycosylation sites (N-X-S/T-X), where X represents every amino acid except for Pro, were located using a Python script. N1 2009 pandemic-like amino acid numbering was used for both N1 and N2, the head domain was set to begin at amino acid residue 82, and the stalk was designated amino acid residues 35 to 81. Tetrameric N1 models were created from the A/Michigan/45/2015 primary sequence using SWISS-MODEL (https://swissmodel.expasy.org), based on an available 2009 pandemic-like N1 head domain structure (PDBID entry 5NWE) (59), and the glycans were added *in silico* using Glyprot (http://www.glycosciences.de/modeling/glyprot/php/main.php). The modeled glycan structures were chosen based on previous work (36), with glycan number 9141 (glcp) being used for Asn386 and 8714 (2 glcnac) for all other sites.

ACKNOWLEDGMENTS

We thank Tahir Malik (FDA), Hongquan Wan (FDA), and Daniel Hebert (University of Massachusetts-Amherst) for critically reading the manuscript and offering several helpful suggestions.

This work was supported in part by grants from the Swedish Research Council K2015-57-21980-04-4 and the Carl Trygger Foundation CTS17:111, as well as federal funds from the NIAID, National Institutes of Health, Department of Health and Human Services, under CEIRS contract number HHSN272201400005C.

REFERENCES

1. Mochizuki K, Kagawa T, Numari A, Harris MJ, Itoh J, Watanabe N, Mine T, Arias IM. 2007. Two N-linked glycans are required to maintain the transport activity of the bile salt export pump (ABCB11) in MDCK II cells. Am J Physiol Gastrointest Liver Physiol 292:G818–G828. https://doi.org/10.1152/ajpgi.00415.2006.
2. Hanson SR, Culyba EK, Hsu TL, Wong CH, Kelly JW, Powers ET. 2009. The core trisaccharide of an N-linked glycoprotein intrinsically accelerates folding and enhances stability. Proc Natl Acad Sci U S A 106:3131–3136. https://doi.org/10.1073/pnas.0810318105.
3. Tokhtaeva E, Munson K, Sachs G, Vagin O. 2010. N-glycan-dependent quality control of the Na,K-ATPase beta(2) subunit. Biochemistry 49:3116–3128. https://doi.org/10.1021/bi100115a.
4. Hebert DN, Lamriben L, Powers ET, Kelly JW. 2014. The intrinsic and extrinsic effects of N-linked glycans on glycoproteostasis. Nat Chem Biol 10:902–910. https://doi.org/10.1038/nchembio.1651.
5. Cai X, Thinn AMM, Wang Z, Shan H, Zhu J. 2017. The importance of N-glycosylation on beta3 integrin ligand binding and conformational regulation. Sci Rep 7:4656. https://doi.org/10.1038/s41598-017-04844-w.
6. Ohtsubo K, Takamatsu S, Minowa MT, Yoshida A, Takeuchi M, Marth JD. 2005. Dietary and genetic control of glucose transporter 2 glycosylation promotes insulin secretion in suppressing diabetes. Cell 123:1307–1321. https://doi.org/10.1016/j.cell.2005.09.041.
7. Wang X, Gu J, Ihara H, Miyoshi E, Honke K, Taniguchi N. 2006. Core fucosylation regulates epidermal growth factor receptor-mediated intracellular signaling. J Biol Chem 281:2572–2577. https://doi.org/10.1074/jbc.M510893200.
8. Goetze AM, Liu YD, Zhang Z, Shah B, Lee E, Bondarenko PV, Flynn GC. 2011. High-mannose glycans on the Fc region of therapeutic IgG antibodies increase serum clearance in humans. Glycobiology 21:949–959. https://doi.org/10.1093/glycob/cwr027.
9. Liu L. 2015. Antibody glycosylation and its impact on the pharmacokinetics and pharmacodynamics of monoclonal antibodies and Fc-fusion proteins. J Pharm Sci 104:1866–1884. https://doi.org/10.1002/jps.24444.
10. Hebert DN, Foellmer B, Helenius A. 1995. Glucose trimming and reglucosylation determine glycoprotein association with calnexin in the endoplasmic reticulum. Cell 81:425–433. https://doi.org/10.1016/0092-8674(95)90395-x.
11. Shi X, Elliott RM. 2004. Analysis of N-linked glycosylation of hantaan virus glycoproteins and the role of oligosaccharide side chains in protein folding and intracellular trafficking. J Virol 78:5414–5422. https://doi.org/10.1128/jvi.78.10.5414-5422.2004.
12. Braakman I, van Anken E. 2000. Folding of viral envelope glycoproteins in the endoplasmic reticulum. Traffic 1:533–539. https://doi.org/10.1034/j.1600-0854.2000.010702.x.
13. Skehel JJ, Stevens DJ, Daniels RS, Douglas AR, Knossow M, Wilson IA, Wiley DC. 1984. A carbohydrate side chain on hemagglutinins of Hong Kong influenza viruses inhibits recognition by a monoclonal antibody. Proc Natl Acad Sci U S A 81:1779–1783. https://doi.org/10.1073/pnas.81.6.1779.
14. Wei X, Decker JM, Wang S, Hui H, Kappes JC, Wu X, Salazar-Gonzalez JF, Salazar MG, Kilby JM, Saag MS, Komarova NL, Nowak MA, Hahn BH,

Kwong PD, Shaw GM. 2003. Antibody neutralization and escape by HIV-1. Nature 422:307–312. https://doi.org/10.1038/nature01470.
15. Lennemann NJ, Rhein BA, Ndungo E, Chandran K, Qiu X, Maury W. 2014. Comprehensive functional analysis of N-linked glycans on Ebola virus GP1. mBio 5:e00862-13. https://doi.org/10.1128/mBio.00862-13.
16. Walls AC, Tortorici MA, Frenz B, Snijder J, Li W, Rey FA, DiMaio F, Bosch BJ, Veesler D. 2016. Glycan shield and epitope masking of a coronavirus spike protein observed by cryo-electron microscopy. Nat Struct Mol Biol 23:899–905. https://doi.org/10.1038/nsmb.3293.
17. Wan H, Gao J, Yang H, Yang S, Harvey R, Chen YQ, Zheng NY, Chang J, Carney PJ, Li X, Plant E, Jiang L, Couzens L, Wang C, Strohmeier S, Wu WW, Shen RF, Krammer F, Cipollo JF, Wilson PC, Stevens J, Wan XF, Eichelberger MC, Ye Z. 2019. The neuraminidase of A(H3N2) influenza viruses circulating since 2016 is antigenically distinct from the A/Hong Kong/4801/2014 vaccine strain. Nat Microbiol 4:2216–2225. https://doi.org/10.1038/s41564-019-0522-6.
18. Hebert DN, Zhang JX, Chen W, Foellmer B, Helenius A. 1997. The number and location of glycans on influenza hemagglutinin determine folding and association with calnexin and calreticulin. J Cell Biol 139:613–623. https://doi.org/10.1083/jcb.139.3.613.
19. Daniels R, Kurowski B, Johnson AE, Hebert DN. 2003. N-linked glycans direct the cotranslational folding pathway of influenza hemagglutinin. Mol Cell 11:79–90. https://doi.org/10.1016/s1097-2765(02)00821-3.
20. Molinari M, Eriksson KK, Calanca V, Galli C, Cresswell P, Michalak M, Helenius A. 2004. Contrasting functions of calreticulin and calnexin in glycoprotein folding and ER quality control. Mol Cell 13:125–135. https://doi.org/10.1016/s1097-2765(03)00494-5.
21. Wang N, Glidden EJ, Murphy SR, Pearse BR, Hebert DN. 2008. The cotranslational maturation program for the type II membrane glycoprotein influenza neuraminidase. J Biol Chem 283:33826–33837. https://doi.org/10.1074/jbc.M806897200.
22. Gamblin SJ, Skehel JJ. 2010. Influenza hemagglutinin and neuraminidase membrane glycoproteins. J Biol Chem 285:28403–28409. https://doi.org/10.1074/jbc.R110.129809.
23. Yoon SW, Webby RJ, Webster RG. 2014. Evolution and ecology of influenza A viruses. Curr Top Microbiol Immunol 385:359–375. https://doi.org/10.1007/82_2014_396.
24. Morens DM, Taubenberger JK, Fauci AS. 2009. The persistent legacy of the 1918 influenza virus. N Engl J Med 361:225–229. https://doi.org/10.1056/NEJMp0904819.
25. Rajao DS, Vincent AL, Perez DR. 2018. Adaptation of human influenza viruses to swine. Front Vet Sci 5:347. https://doi.org/10.3389/fvets.2018.00347.
26. Wang H, Dou D, Östbye H, Revol R, Daniels R. 2019. Structural restrictions for influenza neuraminidase activity promote adaptation and diversification. Nat Microbiol 4:2565–2577. https://doi.org/10.1038/s41564-019-0537-z.
27. Bos TJ, Davis AR, Nayak DP. 1984. NH2-terminal hydrophobic region of influenza virus neuraminidase provides the signal function in translocation. Proc Natl Acad Sci U S A 81:2327–2331. https://doi.org/10.1073/pnas.81.8.2327.
28. Paterson RG, Lamb RA. 1990. Conversion of a class II integral membrane protein into a soluble and efficiently secreted protein: multiple intracellular and extracellular oligomeric and conformational forms. J Cell Biol 110:999–1011. https://doi.org/10.1083/jcb.110.4.999.
29. Bucher DJ, Kilbourne ED. 1972. A 2 (N2) neuraminidase of the X-7 influenza virus recombinant: determination of molecular size and subunit composition of the active unit. J Virol 10:60–66. https://doi.org/10.1128/JVI.10.1.60-66.1972.
30. Varghese JN, Laver WG, Colman PM. 1983. Structure of the influenza virus glycoprotein antigen neuraminidase at 2.9 A resolution. Nature 303:35–40. https://doi.org/10.1038/303035a0.
31. Dou D, Revol R, Östbye H, Wang H, Daniels R. 2018. Influenza A virus cell entry, replication, virion assembly and movement. Front Immunol 9:1581. https://doi.org/10.3389/fimmu.2018.01581.
32. Colman PM, Varghese JN, Laver WG. 1983. Structure of the catalytic and antigenic sites in influenza virus neuraminidase. Nature 303:41–44. https://doi.org/10.1038/303041a0.
33. Nordholm J, da Silva DV, Damjanovic J, Dou D, Daniels R. 2013. Polar residues and their positional context dictate the transmembrane domain interactions of influenza a neuraminidases. J Biol Chem 288:10652–10660. https://doi.org/10.1074/jbc.M112.440230.
34. Dou D, da Silva DV, Nordholm J, Wang H, Daniels R. 2014. Type II transmembrane domain hydrophobicity dictates the cotranslational dependence for inversion. Mol Biol Cell 25:3363–3374. https://doi.org/10.1091/mbc.E14-04-0874.
35. Nordholm J, Petitou J, Ostbye H, da Silva DV, Dou D, Wang H, Daniels R. 2017. Translational regulation of viral secretory proteins by the 5′ coding regions and a viral RNA-binding protein. J Cell Biol 216:2283–2293. https://doi.org/10.1083/jcb.201702102.
36. She YM, Farnsworth A, Li X, Cyr TD. 2017. Topological N-glycosylation and site-specific N-glycan sulfation of influenza proteins in the highly expressed H1N1 candidate vaccines. Sci Rep 7:10232. https://doi.org/10.1038/s41598-017-10714-2.
37. da Silva DV, Nordholm J, Madjo U, Pfeiffer A, Daniels R. 2013. Assembly of subtype 1 influenza neuraminidase is driven by both the transmembrane and head domains. J Biol Chem 288:644–653. https://doi.org/10.1074/jbc.M112.424150.
38. da Silva DV, Nordholm J, Dou D, Wang H, Rossman JS, Daniels R. 2015. The influenza virus neuraminidase protein transmembrane and head domains have coevolved. J Virol 89:1094–1104. https://doi.org/10.1128/JVI.02005-14.
39. Saito T, Taylor G, Webster RG. 1995. Steps in maturation of influenza A virus neuraminidase. J Virol 69:5011–5017. https://doi.org/10.1128/JVI.69.8.5011-5017.1995.
40. Sun S, Wang Q, Zhao F, Chen W, Li Z. 2011. Glycosylation site alteration in the evolution of influenza A (H1N1) viruses. PLoS One 6:e22844. https://doi.org/10.1371/journal.pone.0022844.
41. Sun S, Wang Q, Zhao F, Chen W, Li Z. 2012. Prediction of biological functions on glycosylation site migrations in human influenza H1N1 viruses. PLoS One 7:e32119. https://doi.org/10.1371/journal.pone.0032119.
42. Kim P, Jang YH, Kwon SB, Lee CM, Han G, Seong BL. 2018. Glycosylation of hemagglutinin and neuraminidase of influenza A virus as signature for ecological spillover and adaptation among influenza reservoirs. Viruses 10:183. https://doi.org/10.3390/v10040183.
43. Shakin-Eshleman SH, Spitalnik SL, Kasturi L. 1996. The amino acid at the X position of an Asn-X-Ser sequon is an important determinant of N-linked core-glycosylation efficiency. J Biol Chem 271:6363–6366. https://doi.org/10.1074/jbc.271.11.6363.
44. Mellquist JL, Kasturi L, Spitalnik SL, Shakin-Eshleman SH. 1998. The amino acid following an asn-X-Ser/Thr sequon is an important determinant of N-linked core glycosylation efficiency. Biochemistry 37:6833–6837. https://doi.org/10.1021/bi972217k.
45. Eichelberger MC, Wan H. 2015. Influenza neuraminidase as a vaccine antigen. Curr Top Microbiol Immunol 386:275–299. https://doi.org/10.1007/82_2014_398.
46. Mitnaul LJ, Matrosovich MN, Castrucci MR, Tuzikov AB, Bovin NV, Kobasa D, Kawaoka Y. 2000. Balanced hemagglutinin and neuraminidase activities are critical for efficient replication of influenza A virus. J Virol 74:6015–6020. https://doi.org/10.1128/jvi.74.13.6015-6020.2000.
47. Kaverin NV, Matrosovich MN, Gambaryan AS, Rudneva IA, Shilov AA, Varich NL, Makarova NV, Kropotkina EA, Sinitsin BV. 2000. Intergenic HA-NA interactions in influenza A virus: postreassortment substitutions of charged amino acid in the hemagglutinin of different subtypes. Virus Res 66:123–129. https://doi.org/10.1016/s0168-1702(99)00131-8.
48. Kaverin NV, Gambaryan AS, Bovin NV, Rudneva IA, Shilov AA, Khodova OM, Varich NL, Sinitsin BV, Makarova NV, Kropotkina EA. 1998. Postreassortment changes in influenza A virus hemagglutinin restoring HA-NA functional match. Virology 244:315–321. https://doi.org/10.1006/viro.1998.9119.
49. Wagner R, Matrosovich M, Klenk HD. 2002. Functional balance between haemagglutinin and neuraminidase in influenza virus infections. Rev Med Virol 12:159–166. https://doi.org/10.1002/rmv.352.
50. Lavie M, Hanoulle X, Dubuisson J. 2018. Glycan shielding and modulation of hepatitis C virus neutralizing antibodies. Front Immunol 9:910. https://doi.org/10.3389/fimmu.2018.00910.
51. Quinones-Kochs MI, Buonocore L, Rose JK. 2002. Role of N-linked glycans in a human immunodeficiency virus envelope glycoprotein: effects on protein function and the neutralizing antibody response. J Virol 76:4199–4211. https://doi.org/10.1128/jvi.76.9.4199-4211.2002.
52. Leemans A, Boeren M, Van der Gucht W, Pintelon I, Roose K, Schepens B, Saelens X, Bailey D, Martinet W, Caljon G, Maes L, Cos P, Delputte P. 2018. Removal of the N-glycosylation sequon at position N116 located in p27 of the respiratory syncytial virus fusion protein elicits enhanced antibody responses after DNA immunization. Viruses 10:426. https://doi.org/10.3390/v10080426.
53. Gao J, Couzens L, Eichelberger MC. 2016. Measuring influenza neuraminidase inhibition antibody titers by enzyme-linked lectin assay. J Vis Exp 2016:54573. https://doi.org/10.3791/54573.

54. Hoffmann E, Neumann G, Kawaoka Y, Hobom G, Webster RG. 2000. A DNA transfection system for generation of influenza A virus from eight plasmids. Proc Natl Acad Sci U S A 97:6108–6113. https://doi.org/10.1073/pnas.100133697.
55. Mellroth P, Daniels R, Eberhardt A, Ronnlund D, Blom H, Widengren J, Normark S, Henriques-Normark B. 2012. LytA, major autolysin of Streptococcus pneumoniae, requires access to nascent peptidoglycan. J Biol Chem 287:11018–11029. https://doi.org/10.1074/jbc.M111.318584.
56. Sandbulte MR, Gao J, Straight TM, Eichelberger MC. 2009. A miniaturized assay for influenza neuraminidase-inhibiting antibodies utilizing reverse genetics-derived antigens. Influenza Other Respir Viruses 3:233–240. https://doi.org/10.1111/j.1750-2659.2009.00094.x.
57. Reed LJ, Muench H. 1938. A simple method of estimating fifty percent end points. Am J Epidemiol 27:493–497. https://doi.org/10.1093/oxfordjournals.aje.a118408.
58. Bao Y, Bolotov P, Dernovoy D, Kiryutin B, Zaslavsky L, Tatusova T, Ostell J, Lipman D. 2008. The influenza virus resource at the National Center for Biotechnology Information. J Virol 82:596–601. https://doi.org/10.1128/JVI.02005-07.
59. Pokorná J, Pachl P, Karlukova E, Hejdánek J, Řezáčová P, Machara A, Hudlický J, Konvalinka J, Kožíšek M. 2018. Kinetic, thermodynamic, and structural analysis of drug resistance mutations in neuraminidase from the 2009 pandemic influenza virus. Viruses 10:339. https://doi.org/10.3390/v10070339.